Available online at www.sciencedirect.com

SciVerse ScienceDirect

Ceramics International 38 (2012) 1785–1791

CERAMICS INTERNATIONAL

www.elsevier.com/locate/ceramint

Electrical properties of $(La_{0.9}Ca_{0.1})(Co_{1-x}Ni_x)O_{3-\delta}$ cathode materials for SOFCs

T.H. Hsieh [a], F.H. Jhong [b], D.T. Ray [a], Y.P. Fu [b,*]

[a] Department of Resources Engineering, National Cheng Kung University, Tainan 70101, Taiwan, ROC

[b] Department of Material Science and Engineering, National Dong-Hwa University, Shou-Feng, Hualien 97401, Taiwan, ROC

Received 30 August 2011; received in revised form 29 September 2011; accepted 30 September 2011

Available online 6 October 2011

Abstract

Modified perovskite ceramics $(La_{0.9}Ca_{0.1})(Co_{1-x}Ni_x)O_{3-\delta}$ ($x = 0$–0.3) cathodes for solid oxide fuel cells (SOFCs) were synthesized by solid state reaction. The lattice parameters, electrical conductivity, activation energy, and microstructures of these specimens were investigated systematically in this study. The results exhibited that all specimens are rhombohedron structures and their tolerance factors were greater than 0.97, indicating that the perovskite was not distorted by Ni^{2+} cation substitution for the B site of $(La_{0.9}Ca_{0.1})CoO_{3-\delta}$. The microstructures of the $(La_{0.9}Ca_{0.1})(Co_{1-x}Ni_x)O_{3-\delta}$ specimens showed good densification, and were well-sintered, with few pores. The electrical conductivity behavior conformed to the nature of a semiconductor, for all specimens. As $x = 0.1$, the electrical conductivity reached the maximum value of 750.3 S/cm at 800 °C, and the activation energy calculated from the Arrhenius plot of the electrical conductivity versus the reciprocal of temperature is 7.1 kJ/mol.

The novelty of this study is its introduction of the concept of defect chemistry to explain the relationship between compensation mechanisms and electrical conductivity. The information gleaned regarding charge compensation mechanisms and defect formation may be valuable for a better understanding of the cathode of $(La_{0.9}Ca_{0.1})(Co_{1-x}Ni_x)O_{3-\delta}$ ceramics used for SOFCs. Moreover, the information about oxygen content versus temperature is useful for expressing the relationship between electrical conductivity and composition. Therefore, we also used thermogravimetric analysis combined with the room-temperature oxygen content which was determined by iodometric titration to investigate the oxygen content from room temperature to high temperature, in air. Based on the experimental results, the $(La_{0.9}Ca_{0.1})(Co_{0.9}Ni_{0.1})O_{3-\delta}$ specimen shows high electrical conductivity. Consequently, it is identified as a promising candidate for cathode SOFC applications.

Keywords: A. Powders: solid state reaction; C. Electrical conductivity; D. Perovskites; E. Fuel cells; E. Electrodes

1. Introduction

Solid oxide fuel cells (SOFCs) offer an environmentally friendly alternative to heat engines for generating electrical power, owing to their high energy conversion efficiency and low emission of air pollution [1,2]. Generally, yttria-stabilized zirconia (YSZ) is a well-known material used as the electrolyte, and strontium-doped lanthanum manganite (LSM) is a common material used as the cathode for SOFCs. However, the above-mentioned materials required a high operating temperature (~1000 °C) in order to offer sufficient ionic and electrical conductivities [3,4]. Such a high temperature will bring about some serious problems. For example, if an interfacial reaction occurred between a LSM cathode and a YSZ electrolyte, resulting in insulating phases. The formation of intermediate phases between LSM and YSZ in the interface has been observed in the previous literatures [5–8]. These intermediate phases such as $SrZrO_3$, can significantly degrade the performance of SOFCs due to their low ionic conductivity compared with that of YSZ [5,9]. Furthermore, ceramic-based interconnect materials with high costs are required to tolerate the high operating temperatures [10].

To resolve above-mentioned drawbacks, it is important to find new electrolyte and cathode materials for SOFCs, which can operated at intermediate temperature (600–800 °C). Recently, electrolyte materials such as gadolinia-doped ceria

* Corresponding author. Tel.: +886 3 8634209; fax: +886 3 8634200.
E-mail address: d887503@alumni.nthu.edu.tw (Y.P. Fu).

0272-8842/$36.00
doi:10.1016/j.ceramint.2011.09.065

(GDC) and samaria-doped ceria (SDC) have been widely studied because their ionic conductivities are higher than that of YSZ at an intermediate temperature range (600–800 °C) [11]. On the other hand, cathode materials with high mixed ionic and electronic conductivities are also promising candidates. The cobalt-contained perovskites are potential candidates for cathode materials for SOFCs due to their high electrical and ionic conductivities and their excellent electrochemical properties. Base on the above-mentioned reasons, we set out to develop a new cathode material with a stable perovskite structure and high electrical conductivity. In this study, perovskite-type ceramics, $(La_{0.9}Ca_{0.1})(Co_{1-x}Ni_x)O_{3-\delta}$ ($x = 0.0$–0.3) were systematically investigated and evaluated for use as a possible cathode material for SOFCs. Moreover, the concept of defect chemistry is introduced to explain the relationship between the compensation mechanisms and the electrical conductivity.

2. Experimental

2.1. Sample preparation

The $(La_{0.9}Ca_{0.1})(Co_{1-x}Ni_x)O_{3-\delta}$ hereafter refer to LCCN were synthesized by conventional solid-state reaction. The starting materials were A.R. grade of La_2O_3, $CaCO_3$, NiO and Co_3O_4 powders (>99.9%). Stoichiometric amount of the starting materials were mixed and ball-milled for 12 h using ethanol as medium. Then these powders were dried at 80 °C in an oven and calcined at 1000 °C for 12 h to obtain the anticipated perovskite phase. The calcined LCCN powders were pelletized with a small amount of PVA as binder. The powder samples were applied an uniaxial pressure of 250 MPa with the dimensions of 10 mm in length, 5 mm in width, and 5 mm in height. Rectangular bar specimens were then finally sintered at 1400 °C in air for 6 h with a programmed heating rate of 5 °C/min and cooling rate of 3 °C/min. The sintered samples were over 92% of theoretical density for LCCN specimens.

2.2. Characterization

A computer-interface X-ray diffractometer (XRD; Rigaku D/MAX-2500V) with Cu Kα radiation (1.5418 Å) was used to identify the crystalline phase and to determine the lattice parameters, which recorded with scanning rate of 4°/min and scanning range 20–80°. The microstructure and surface morphological were observed by scanning electron microscope (SEM, Hitachi 3500H). The chemical composition of the LCCN was analyzed by energy dispersive X-ray spectroscopy (EDS). The average grain size, G_a was calculated using the following relation:

$$G_a = \frac{1.5 \times L}{M \times N} \tag{1}$$

where 1.5 is a geometry-dependent proportionality constant [12], L is the total length of testing lines, M is the magnification and N is the total number of intercepts of grain boundaries. The electrical conductivity measurements were made at various temperatures in the range 300–850 °C in air with the interval of 50 °C by the direct current (DC) four-terminal technique. Four Pt leads were attached to the sample with Pt paste and fired at 800 °C. The electrical conductivities were calculation by following equation:

$$\sigma = \frac{L \times I}{A \times \Delta V} \tag{2}$$

where σ is the electrical conductivity, L is the distance between two contact points, I is the fixed current, A is the area of cross section and ΔV is the difference of measured voltage between two probes. Arrhenius plots ($\ln(\sigma T)$ versus $10^3/T$) were constructed, and activation energies for conduction were computed. Activation energy for conduction is obtained by plotting the ionic conductivity data in the Arrhenius relation for thermally activated conduction. It was calculated according to the following equation:

$$\sigma T = \sigma_o \exp\left(-\frac{E_a}{kT}\right) \tag{3}$$

where E_a is the activation energy for conduction, T is absolute temperature, and σ_o is a pre-exponential factor. Thermogravimetric analysis (TGA, TG–DTA/DSC Setaram, Caluiro) was performed on calcined powder specimens using a heating rate of 10 °C/min to study oxygen stoichiometry. Room temperature oxygen stoichiometry of calcined powder specimens was determined by iodometric titration [13,14].

3. Results and discussion

3.1. Crystal structures and surface morphologies

The XRD patterns of sintered LCCN specimens are presented in Fig. 1. The introduction of Ni^{2+} cation substitution for the B-site of $(La_{0.9}Ca_{0.1})CoO_{3-\delta}$ can cause a small shift in the diffraction peaks. The lattice parameters and tolerance

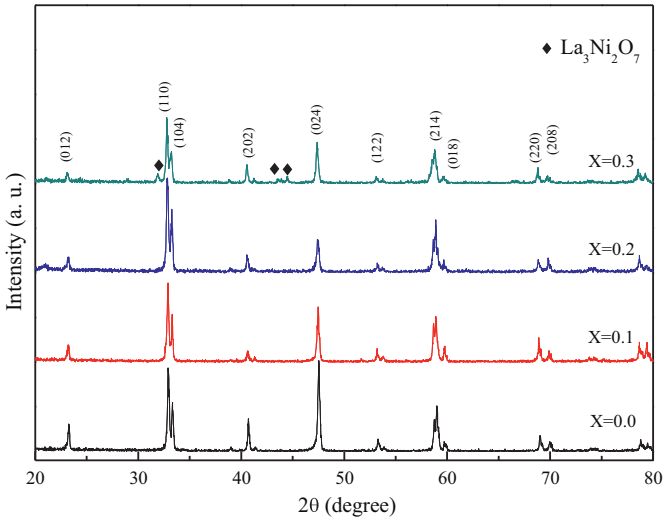

Fig. 1. X-ray diffraction patterns of $(La_{0.9}Ca_{0.1})(Co_{1-x}Ni_x)O_{3-\delta}$ sintered at 1400 °C for 6 h.

Table 1
Lattice parameters, tolerance factors (t^*), average grain sizes and apparent densities for $(La_{0.9}Ca_{0.1})(Co_{1-x}Ni_x)O_{3-\delta}$ specimens.

Specimens	Lattice parameters (nm)		t^*	Average grain size (μm)	Apparent density (g/cm^3)
	a	c			
$x = 0.0$	5.4384	13.0836	1.000	23.5	6.45
$x = 0.1$	5.4517	13.1366	0.993	62.2	6.54
$x = 0.2$	5.4586	13.1371	0.986	88. 7	6.46
$x = 0.3$	5.4659	13.1817	0.979	105.5	6.77

factors of the LCCN specimens are listed in Table 1. The results indicate that the introduction of Ni^{2+} substitution for Co^{3+} causes a swell in lattice parameters. This is due to the fact that the ionic radius of Ni^{2+} is 0.069 nm, which is larger than one of Co^{3+} is 0.055 nm. With an increase in the substitution of Ni^{2+} amounts, the lattice constants of a and b are increased, behavior which corresponds with Robert's report [15]. As compared with JCPDS data (powder diffraction file No. 36-1388), results clearly showed that the main crystal structure for LCCN was a rhombohedra perovskite structure for $x = 0.0$–0.2. However, for $x = 0.3$ the XRD pattern appears a secondary phase of $La_3Ni_2O_7$. To evaluate the stability of forming the perovskite structure, we calculated the values of the tolerance factor. The formula for calculating the tolerance factor (t^*) is shown in the following equation:

$$t* = \frac{R_A + R_O}{\sqrt{2}(R_B + R_O)} \tag{4}$$

where R_A, R_B and R_O are the ionic radii of A, B and O in the ABO_3 perovskite, respectively. As the value of t^* locates in the range of 0.8–1.0, this means that the perovskite structure is sustainable [16]. In a typical perovskite structure, the A-site has 12 coordinate ions, while the B-site and oxygen sites both have 6 coordinate ions, respectively. In this study, the ionic radii of La^{3+} and Ca^{2+} with a coordination number of 12 are 0.136 nm and 0.134 nm, respectively; the ionic radii of Ni^{2+} and Co^{3+} with a coordination number of 6 are 0.069 nm and 0.055 nm, respectively; and the radius of oxygen ion O^{2-} is 0.126 nm [17]. The values of t^* varied from 1.000 for $(La_{0.9}Ca_{0.1})CoO_{3-\delta}$ to 0.979 for $(La_{0.9}Ca_{0.1})(Co_{0.7}Ni_{0.3})O_{3-\delta}$, indicating that the value of t^* decreased with an increase in the substitution amount of Ni for LCCN specimens, as shown in Table 1. The tolerance factors for all specimens are larger than 0.97, indicating that the perovskite structure does not distort via Ni^{2+} substitution for Co^{3+} in the B-site of LCCN.

The surface morphologies are shown in Fig. 2, with results indicating that no matter what the amount of nickel substitution, the microstructures of the LCCNs revealed good densification and were well-sintered, with few pores. All specimens were over 92% of the theoretical density, as presented in Table 1. It is noticeable that little precipitation appeared along the grain boundaries for $(La_{0.9}Ca_{0.1})CoO_{3-\delta}$ as shown in Fig. 3. In light of the surface EDS result, it is clearly observed that the precipitation consisted of a higher Ca content than that of the stoichiometric composition. However, no clear precipitation appeared in the other compositions for $x = 0.1$–0.3. This result implied that the Ni^{2+} substituted for Co^{3+} formed a solid solution for LCCN ceramics. The grain size varied from 23.5 μm for $(La_{0.9}Ca_{0.1})CoO_{3-\delta}$ to 105.5 μm for $(La_{0.9}Ca_{0.1})(Co_{0.7}Ni_{0.3})O_{3-\delta}$, the grain size increased with increasing Ni content for the LCCN specimens, as listed in Table 1. The rate of grain growth is taken to be approximately equal to the grain boundary velocity, so that:

$$V_b \approx \frac{dG}{dt} = M_b F_b \tag{5}$$

where M_b is the boundary mobility and F_b is the driving force for boundary migration [18]. In many analyses, the driving force is taken as the pressure difference across the boundary:

$$F_b = \frac{\alpha \gamma_{gb}}{G} \tag{6}$$

where γ_{gb} is the specific grain boundary energy, α is a geometrical constant that depends on the shape of the boundary, and G is the grain size. The grain boundary velocity V_b is given by

$$V_b \approx \frac{dG}{dt} = M_b\left(\frac{\alpha \gamma_{gb}}{G}\right) \tag{7}$$

Upon integrating Eq. (7) we have

$$G^2 - G_0^2 = 2\alpha M_b \gamma_{gb} t \tag{8}$$

where G_0 is the initial size. Eq. (8) is suitable for a fixed temperature. Assuming the grain boundary energy γ_{gb} and geometrical constant α are both fixed, the rate of grain growth is proportional to the boundary mobility M_b. However, the boundary mobility is given by the mobility of atoms moving across the boundary divided by the number of atoms involved per unit area of grain boundary $M_b = (D_a/kT)(\Omega/\delta_{gb})$ where Ω is the atomic volume and δ is the boundary thickness. Since both Boltzmann's constant k and boundary thickness δ (~0.5 nm) are constant at a fixed temperature, M_b depends on the diffusion coefficient D_a and the atomic volume Ω. For ceramics, in which both cations and anions must diffuse, D_a represents the diffusion coefficient of the slowest species. As stated above, with increasing the Ni-doping level, the grain size is gradually increased. In this study, the stoichiometric variation is only observed in the Co to Ni ratio for $(La_{0.9}Ca_{0.1})(Co_{1-x}Ni_x)O_{3-\delta}$ specimens. Based on the fact that M_b is proportional to the diffusivity of the slowest species (D_b) and its atomic volume (Ω), it is suspected that the limiting diffusivity D_b is the diffusion coefficient of Co in $(La_{0.9}Ca_{0.1})(Co_{1-x}Ni_x)O_{3-\delta}$. With increasing Ni-doping levels, the atomic volume (Ω) of Co is reduced. The increase in M_b results in the increase in grain size.

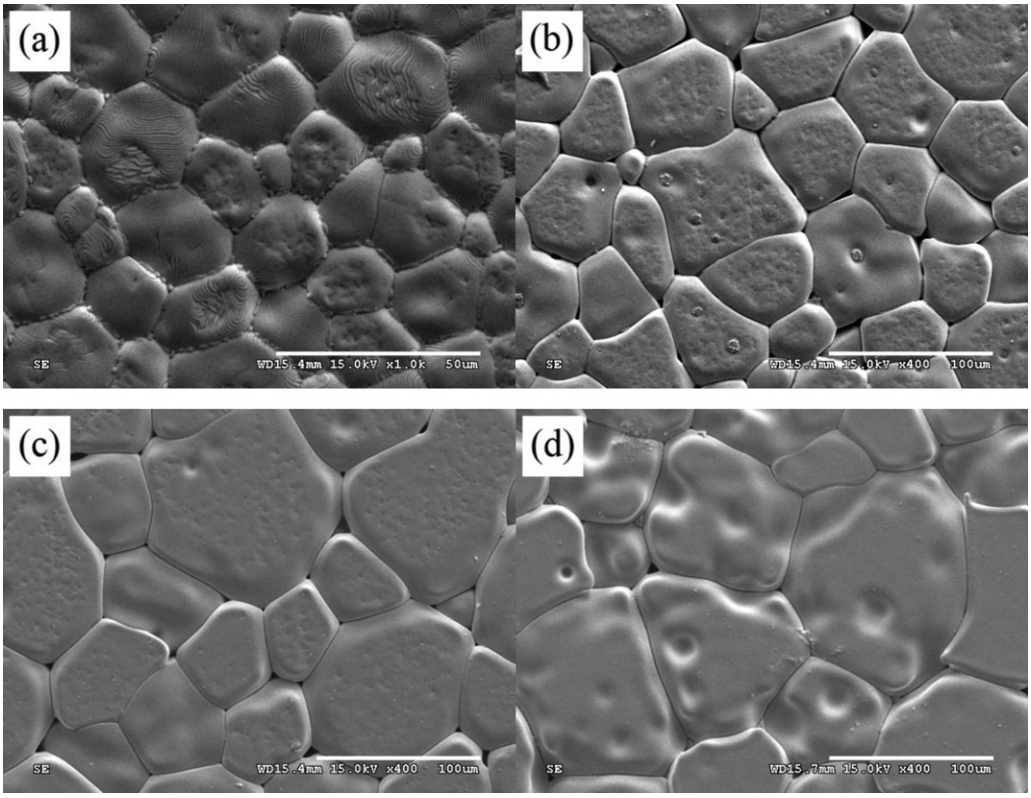

Fig. 2. SEM images of surface microstructures for $(La_{0.9}Ca_{0.1})(Co_{1-x}Ni_x)O_{3-\delta}$: (a) $x = 0.0$, (b) $x = 0.1$, (c) $x = 0.2$ and (d) $x = 0.3$ sintered at 1400 °C for 6 h.

On the basis of (1) the rate of grain growth being proportional to the boundary mobility M_b, and (2) the experiment results regarding the grain size (from SEM images), we thus conclude that the introduction of Ni^{2+} into Co^{3+} can significantly enhance grain growth in LCCN specimens.

3.2. Electrical conductivities

The Arrhenius plot for the electrical conductivity of $(La_{0.9}Ca_{0.1})(Co_{1-x}Ni_x)O_{3-\delta}$ specimens in air is plotted in Fig. 4. With increasing temperature, the hopping of small polarons increases. Consequently, the electrical conductivities increase at high temperatures in all specimens, implying that the electrical conduction occurs by thermally activated of small polarons hopping [19]. The electrical conductivity and activity energy values are listed in Table 2. In light of the electrical conductivity results, it was found that $(La_{0.9}Ca_{0.1})(Co_{0.9}Ni_{0.1})O_{3-\delta}$ had the maximum conductivity value ($\sigma_{800\,^\circ C} = 750.3$ S/cm) and the minimum activation energy ($E_a = 7.1$ kJ/mol). However, for $x = 0.3$, the $(La_{0.9}Ca_{0.1})(Co_{0.7}Ni_{0.3})O_{3-\delta}$ specimen revealed the minimum electrical conductivity value ($\sigma_{850\,^\circ C} = 102.4$ S/cm) and the maximum activation energy ($E_a = 13.1$ kJ/mol) compared with all specimens. This may be due to the appearance of the secondary phase of $La_3Ni_2O_7$ with low electrical conductivity. The electrical conductivities of $(La_{0.9}Ca_{0.1})(Co_{1-x}Ni_x)O_{3-\delta}$ at a temperature of 800 °C are ranked as follows: $x = 0.1 > x = 0.2 > x = 0.0 > x = 0.3$. As the nickel amount increases, the electrical conductivities are decreased. The $(La_{0.9}Ca_{0.1})CoO_{3-\delta}$ specimen revealed some precipitations appeared along the grain boundaries, resulting in the reduction in the electrical conductivity.

In this study, the concept of defect chemistry is used to explain the mechanism of electrical conductivity, and is discussed as follows. When CaO is dissolved substitutionally into the A (La)-site of $LaCoO_3$, it must be charge-compensated by a defect with a positive effective charge. Two possible defect chemical reactions can be expressed as:

$$CaO + O_2(g) \overset{LaCoO_3}{\longrightarrow} Ca'_{La} + 3O_O + h^\bullet \tag{9}$$

and

$$CaO + O_2(g) \overset{LaCoO_3}{\longrightarrow} Ca'_{La} + \frac{5}{2}O_O + \frac{1}{2}V_O^{\bullet\bullet} \tag{10}$$

The overall electrical conductivity is ascribed to both electronic and ionic compensations. Because $(La_{0.0}Ca_{0.1})CoO_{3-\delta}$-based ceramics are p-type conductors, the electrical conductivity is given by $\sigma = e\mu p$, where e is the electron charge, μ is the hole mobility, and p is the hole concentration. Obviously, the compensation mechanism is completely dominated by electronic compensation, i.e. Eq. (9) may be correct. Similarly, when NiO is dissolved substitutionally into the B(Co)-site of $(La_{0.9}Ca_{0.1})CoO_3$, it must be charge-compensated by a defect with a positive effective charge. Two possible defect chemical reactions can be expressed as:

$$xNiO \overset{La_{0.9}Ca_{0.1}CoO_3}{\longrightarrow} 0.9La_{La} + 0.1Ca'_{La} + xNi'_{Co} + O_O + (x + 0.1)h^\bullet \tag{11}$$

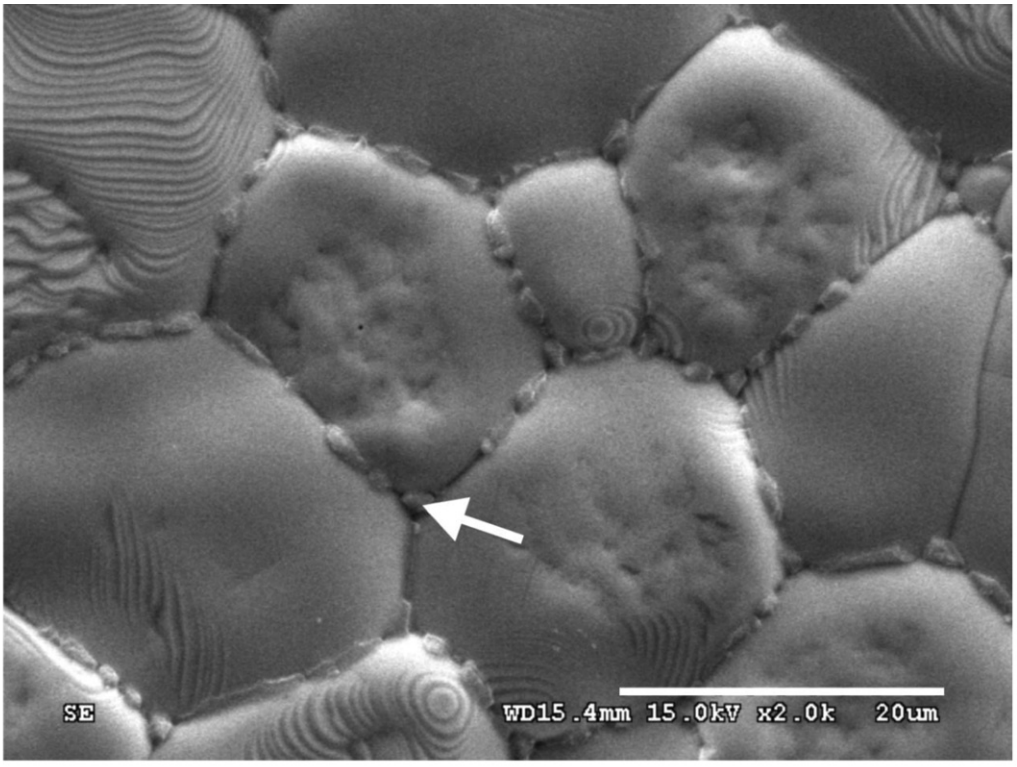

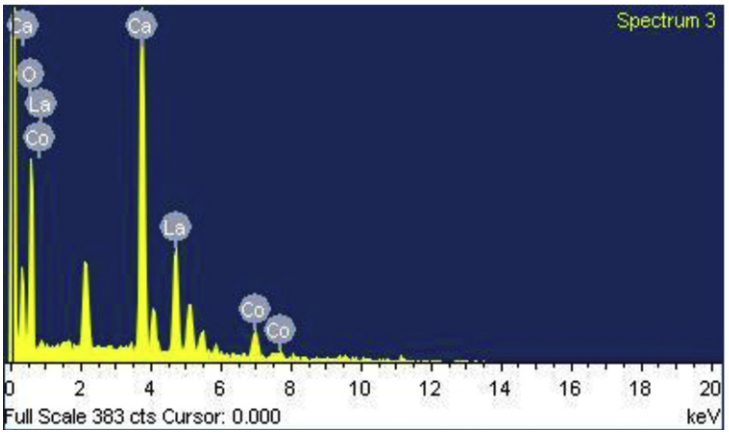

Element	Weight%	Atomic%
O K	25.49	59.26
Ca K	26.38	24.48
Co K	9.26	5.84
La L	38.88	10.41
Totals	100.00	

Fig. 3. EDS spectrum of $(La_{0.9}Ca_{0.1})CoO_{3-\delta}$ on the grain boundaries.

and

$$x\mathrm{NiO} \xrightarrow{\mathrm{La_{0.9}Ca_{0.1}CoO_3}} 0.9\mathrm{La_{La}} + 0.1\mathrm{Ca'_{La}} + x\mathrm{Ni'_{Co}} + 3\mathrm{O_O} + \left(\frac{x+0.1}{2}\right)\mathrm{V_O^{\bullet\bullet}} \quad (12)$$

If the defect chemical reaction is dominated by electronic compensation, the electrical conductivity will be increased with increasing the substitution amount of Ni^{2+} for Co^{3+}. However, electrical conductivity does not increase as per the prediction of chemical defect reaction in Eq. (11). In reality the prevailing compensation mechanism will depend on the Ni-doping level, oxygen activity, and temperature. In this study, the electrical conductivities increased with increasing the Ni-doping level in the range of $x = 0.0$–0.1 for $(La_{0.9}Ca_{0.1})(Co_{1-x}Ni_x)O_{3-\delta}$. We suspected that the compensation mechanism is significantly dominated by electronic compensation for $x = 0.1$. With increasing the x value, the ratio of ionic compensation is gradual increased, and the ratio of electronic compensation shows a gradual reduction for $x = 0.2$–0.3. Moreover, for the composition of $x = 0.3$, precipitation of the secondary phase resulted in the reduction in electrical conductivity. The results suggest that the appropriate amount of Ni substitution for Co in the $(La_{0.9}Ca_{0.1})CoO_{3-\delta}$ specimen will enhance its electrical conductivity. By further increasing the Ni substituting amount, the electrical conductivity is gradually reduced. This phenomenon is due to the change in the ratio of the compensation mechanism.

To further prove the change in the ratio of electronic to ionic compensation with increasing the Ni-doping level, the oxygen contents $(3-\delta)$ of the $(La_{0.9}Ca_{0.1})(Co_{1-x}Ni_x)O_{3-\delta}$ specimens were measured. On the basis of the concept of defect chemistry,

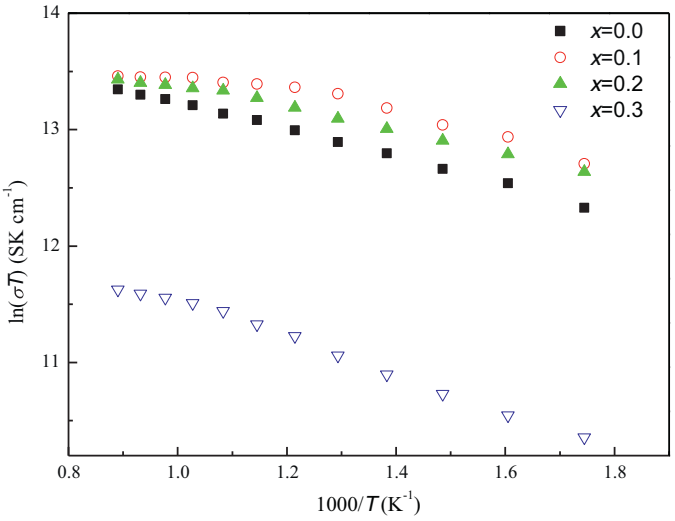

Fig. 4. Arrhenius plots for electrical conductivities of $(La_{0.9}Ca_{0.1})(Co_{1-x}Ni_x)O_{3-\delta}$ in the temperature range from 300 °C to 800 °C.

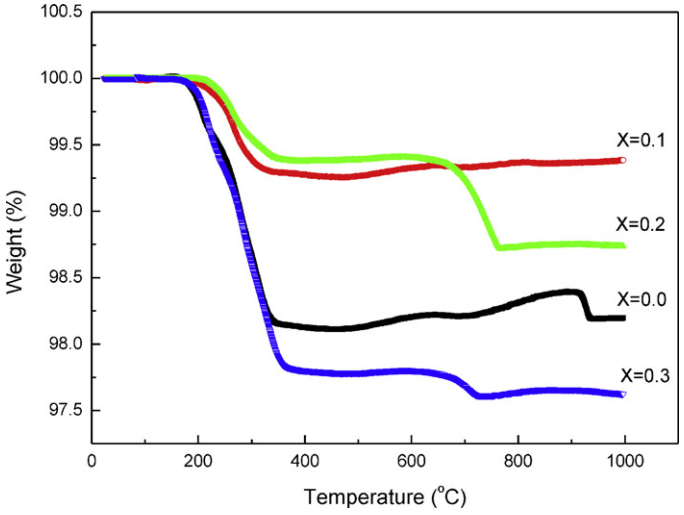

Fig. 5. Relative weight loss as a function of temperature for $(La_{0.9}Ca_{0.1})(Co_{1-x}Ni_x)O_{3-\delta}$ in air.

the decrease in oxygen content implied an increase in ionic compensation. Therefore, we used thermogravimetric analysis to investigate the oxygen content. Measures of the weight losses of $(La_{0.9}Ca_{0.1})(Co_{1-x}Ni_x)O_{3-\delta}$ specimens were performed upon heating them in air, as shown in Fig. 5. With increasing the temperature, the weight loss gradually increased and the magnitude of oxygen loss increased. The magnitude of the weight loss at 800 °C in air can be ranked as follows: $x = 0.03 > x = 0.00 > x = 0.02 > x = 0.01$. This suggests that the B-site acceptor dopant (Ni'_{Co}) plays a substantial role in determining the thermal stability of the lattice oxygen. The weight loss is related to the oxygen loss. By combining the room-temperature oxygen content and the TG weight-loss data (Fig. 5), the oxygen contents for the $(La_{0.9}Ca_{0.1})(Co_{1-x}Ni_x)O_{3-\delta}$ specimens at high temperature in air can be calculated. Oxygen contents $(3-\delta)$ of $(La_{0.9}Ca_{0.1})(Co_{1-x}Ni_x)O_{3-\delta}$ as a function of temperature in air are plotted in Fig. 6. The information regarding oxygen content versus temperature is useful for expressing the relationship between the electrical conductivity and the composition. The compositions with $x = 0.0$ and $x = 0.3$ were found to be significantly oxygen deficient above 370 °C. This suggests that for compositions of $x = 0.0$ and $x = 0.3$, their magnitudes in terms of ionic compensation were significantly increased, and their electrical conductivities were decreased due to the oxygen loss.

Table 2
Electrical conductivities and activation energies of $(La_{0.9}Ca_{0.1})(Co_{1-x}Ni_x)O_{3-\delta}$ specimens at the temperature range of 600–800 °C.

Specimens	Conductivities (S/cm)			E_a (kJ/mol)
	600 °C	700 °C	800 °C	
$x = 0.0$	550.3	556.1	560.9	11.3
$x = 0.1$	645.6	709.8	750.3	7.1
$x = 0.2$	634.8	649.6	665.2	7.9
$x = 0.3$	95.0	100.7	102.4	13.1

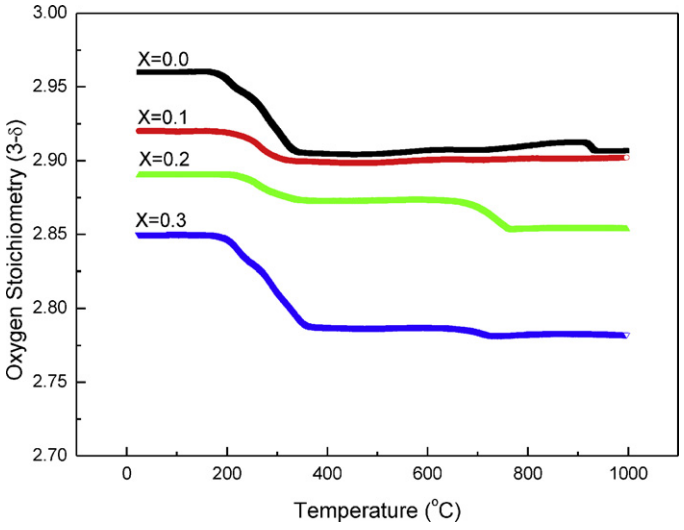

Fig. 6. Oxygen content $(3-\delta)$ of $(La_{0.9}Ca_{0.1})(Co_{1-x}Ni_x)O_{3-\delta}$ as a function of temperature in air.

4. Conclusion

In this study, the lattice parameters, electrical conductivity, activation energy, and microstructure of $(La_{0.9}Ca_{0.1})(Co_{1-x}Ni_x)O_{3-\delta}$ specimens were investigated systematically. The results exhibited that all specimens are rhombohedron structures and their tolerance factors were greater than 0.97, indicating that the perovskite was not distorted with Ni^{2+} cation substitution for the B-site of $(La_{0.9}Ca_{0.1})CoO_{3-\delta}$. The results revealed that the $(La_{0.9}Ca_{0.1})(Co_{0.9}Ni_{0.1})O_{3-\delta}$ specimen possessed the maximum electrical conductivity, $\sigma_{800\ °C} = 750.3$ S/cm along with the minimum activation energy, $E_a = 7.1$ kJ/mol among $(La_{0.9}Ca_{0.1})(Co_{1-x}Ni_x)O_{3-\delta}$ specimens. The electrical conductivities at a temperature of 800 °C for $(La_{0.9}Ca_{0.1})(Co_{1-x}Ni_x)O_{3-\delta}$ were ranked as follows: $x = 0.1 > x = 0.2 > x = 0.0 > x = 0.3$. According to the concept of defect chemistry, it is speculated that the compensation mechanism is significantly

dominated by electronic compensation for $x = 0.1$. With increasing the x value, the ratio of ionic compensation is gradually enlarged, and the ratio of electronic compensation is gradual reduced for $x = 0.2$–0.3. The information regarding oxygen content versus temperature is useful for expressing the relationship between the electrical conductivity and the composition. Therefore, we also used thermogravimetric analysis combined the room-temperature oxygen content to investigate the oxygen content from room temperature to high temperature in air.

The grain size is clearly dependent on the dopant species and grain sizes were distributed in the range of 23.5–105.5 μm for $(La_{0.9}Ca_{0.1})(Co_{1-x}Ni_x)O_{3-\delta}$ specimens. On the basis of (1) the rate of grain growth being proportional to the boundary mobility M_b, and (2) the experiment results regarding grain size (from SEM images), we thus conclude that the introduction of Ni^{2+} into Co^{3+} can significantly enhance grain growth in LCCN specimens. The $(La_{0.9}Ca_{0.1})(Co_{0.9}Ni_{0.1})O_{3-\delta}$ specimen shows high electrical conductivity, which is a promising candidate as a cathode for solid oxide fuel cell (SOFC) applications.

References

[1] M. Mogensen, K.V. Jensen, M.J. Jørgensen, S. Primdahl, Progress in understanding SOFC electrodes, Solid State Ionics 150 (2002) 123–129.

[2] K. Eguchi, Ceramic materials containing rare earth oxides for solid oxide fuel cell, J. Alloys Compd. 250 (1997) 486–491.

[3] C.C. Yang, W.C. Wei, A. Roosen, Electrical conductivity and microstructures of $La_{0.65}Sr_{0.3}MnO_3$—8 mol% yttria-stabilized zirconia, Mater. Chem. Phys. 81 (2003) 134–142.

[4] J. Herle, A.J. Mcevoy, K.R. Thampi, Conductivity measurements of various yttria-stabilized zirconia samples, J. Mater. Sci. 29 (1994) 3691–3701.

[5] S. Faaland, M.A. Einarsrud, K. Wiik, T. Grande, Reactions between $La_{1-x}Ca_xMnO_3$ and CaO-stabilized ZrO_2. Part I. Powder mixtures, J. Mater. Sci. 34 (1999) 957–966.

[6] Y.C. Hsiao, J.R. Selman, The degradation of SOFC electrodes, Solid State Ionics 98 (1997) 33–38.

[7] H. Taimatsu, K. Wada, H. Kaneko, H. Yamamura, Mechanism of reaction between lanthanum manganite and yttria-stabilized zirconia, J. Am. Ceram. Soc. 75 (1992) 401–405.

[8] K. Kleveland, M.A. Einarsrud, C.R. Schmidt, S. Shamsili, S. Faaland, K. Wiik, T. Grande, Reactions between strontium-substituted lanthanum manganite and yttria-stabilized zirconia: II. Diffusion couples, J. Am. Ceram. Soc. 82 (1999) 729–734.

[9] H.Y. Lee, S.M. Oh, Origin of cathodic degradation and new phase formation at the $La_{0.9}Sr_{0.1}MnO_3$/YSZ interface, Solid State Ionics 90 (1996) 133–140.

[10] K. Kendal, S.C. Singhal, High-temperature Solid Oxide Fuel Cells: Fundamentals, Design and Applications. Advanced Technology, Elsevier, London, UK, 2003.

[11] B.C.H. Steele, Appraisal of $Ce_{1-y}Gd_yO_{2-y/2}$ electrolytes for IT-SOFC operation at 500 °C, Solid State Ionics 129 (2000) 95–110.

[12] M.I. Mendelson, Average grain size in polycrystalline ceramics, J. Am. Ceram. Soc. 52 (1969) 443–446.

[13] J.W. Stevenson, T.R. Armstrong, R.D. Carneim, L.R. Pederson, W.J. Weber, Electrical properties of mixed conducting perovskite $La_{1-x}M_xCo_{1-y}Fe_yO_{3-\delta}$ (M = Sr, Ba, Ca), J. Electrochem. Soc. 143 (1996) 2722–2729.

[14] R.J. Nadalin, W.B. Brozda, Chemical method for the determination of the oxidizing (or reducing) powder of certain materials containing a multivalent element in several oxidation states, Anal. Chim. Acta 28 (1963) 282–293.

[15] R. Robert, L. Bocher, B. Sipos, M. Döbeli, A. Weidenkaff, Ni-doped cobaltates as potential materials for high temperature solar thermoelectric converters, Prog. Solid State Chem. 35 (2007) 447–455.

[16] H.H. Zhong, X.L. Zhou, X.Q. Liu, G.Y. Meng, Synthesis and electrical conductivity of perovskite $Gd_{1-x}Ca_xCrO_3$ ($0 < x < 0.3$) by auto-ignition process, Solid State Ionics 176 (2005) 1057–1061.

[17] R.D. Shannon, Revised effective ionic radii and systematic studies of interatomic distances in halides and chalcogenides, Acta Crystallogr. Sect. A Found. Crystallogr. 32 (1976) 751–767.

[18] M.N. Rahaman, Sintering of Ceramics, CRC press, New York, 2008.

[19] I.G. Austin, N.F. Motto, Polarons in crystalline and non-crystalline materials, Adv. Phys. 18 (1969) 41–102.